Low-Density EEG Correction With Multivariate Decomposition and Subspace Reconstruction

Low-density EEG correction with multivariate decomposition and subspace reconstruction

Pasquale Arpaia[1,2], Antonio Esposito[1], Angela Natalizio[3], Marco Parvis[3], Marisa Pesola[1]

***Abstract*— A hybrid method is proposed for removing artifacts from electroencephalographic (EEG) signals. This relies on the integration of artifact subspace reconstruction (ASR) with multivariate empirical mode decomposition. The method can be applied when few EEG sensors are available, a condition in which existing techniques are not effective, and it was tested with two public datasets: (i) semi-synthetic data, and (ii) experimental data with artifacts. One to four EEG sensors were taken into account and the proposal was compared to both ASR and MEMD alone. The proposed method efficiently removed muscular, ocular, or eye-blink artifacts on both semi-synthetic and experimental data. Unexpectedly, the ASR alone also showed compatible performance on semi-synthetic data. However, ASR did not work properly when experimental data were considered. Finally, MEMD was found less effective than both ASR and MEMD-ASR.**

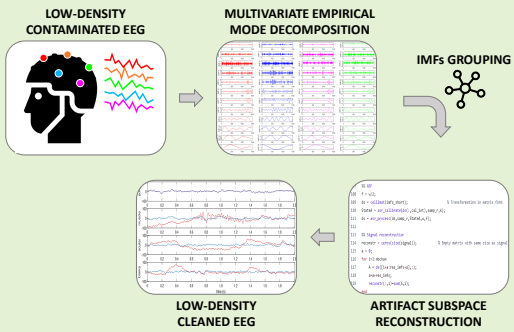

***Index Terms*— electroencephalography, artifact removal, few sensors; empirical mode decomposition, low cost.**

I. Introduction

Electroencephalography (EEG) is a common and consolidated technique for measuring brain activity [1], [2]. The advantages of EEG are ease of use, non-invasiveness, wearability, and low cost [3]–[5]. Thanks to its flexibility, EEG has found application in clinical practice, in research, and in daily life, where a low number of sensors is desirable [6]–[8].

In out-of-the-lab contexts, however, artifacts of both endogenous and exogenous sources contaminate measured EEG signals [9], [10]. Among these, muscular and ocular artifacts are the most common and difficult to face. Artifact removal is essential to obtain a signal reflecting true brain activity, but the choice of a proper removal technique is not obvious, especially with few EEG sensors [11].

A suitable idea is to implement hybrid methods, i.e. combining different rejection/removal techniques. This has been especially proposed for the few EEG sensors case, in an attempt to merge the benefits of different techniques [12]. Several hybrid approaches involve a first step of data decomposition, to produce a higher dimensional signal, and a subsequent artifact removal technique applicable to multi-dimensional signals.

Many approaches rely on empirical mode decomposition (EMD) [13], [14] and its modification [15]. Although these can be employed with simple component selection criteria [16], [17], the integration with techniques like independent component analysis (ICA) [18] or canonical correlation analysis (CCA) [19] led to improved performance compared to single methods. However, they considered signals from multiple sensors decomposed individually.

In recent works, multivariate EMD (i.e., MEMD) was combined with CCA to remove only muscle artifacts from few sensors [20], [21]. It was demonstrated that this hybrid method outperforms multi-channel CCA, but with a higher computational cost. Next, a faster version was proposed [22] by relying on fast MEMD [23]. The approach was only validated on actual EEG with a baseline contaminated by muscle artifacts and further investigation should be carried on.

MEMD was also combined with ICA in removing only ocular artifacts from a five-sensors EEG [24]. An increase in signal-to-noise ratio was shown on both synthetic and experimental data. In [25], wavelet decomposition was applied after ICA on the components recognized as ocular artifacts, in order to preserve most of the actual EEG signal. This method was only tested on experimental data and many sensing channels were needed for applying the ICA.

As a common limitation, the mentioned approaches specifically remove a single artifact type, i.e. either muscular [19]–[22], [26] or ocular [24], [27]–[29] ones. Nonetheless, the artifact removal technique should be applicable to a few-sensor scenario for different types of artifacts, since they can all occur during actual EEG acquisition. Despite its importance, such investigations result still scarce in the few-sensors scenario.

It should be noted that the abovementioned methods combine modal decomposition with blind-source separation tech-

[1] Department of Electrical Engineering and Information Technology (DIETI), Università degli Studi di Napoli Federico II, Naples, Italy
[2] Centro Interdipartimentale di Ricerca in Management Sanitario e Innovazione in Sanità (CIRMIS), Università degli Studi di Napoli Federico II, Naples, Italy
[3] Department of Electronics and Telecommunications (DET), Politecnico di Torino, Turin, Italy
*This work was part of the Project INTENSE, MISE F/310148/01/X56

niques. The latter rely on strict assumptions of independence of components to separate underlying sources [30], which is not always the case for modal decomposition. Instead, an adaptive filter such as the artifact subspace reconstruction (ASR) [31]–[33] has less strict assumptions and it already proved more effective in comparison with other methods [11].

Therefore, a novel hybrid method for artifact removal in low-density EEG setups is proposed. For the first time, the MEMD was combined with ASR to remove artifacts from few available EEG signals and even in single-sensor settings. In particular, Section II provides a background on artifact removal, Section III introduces the proposed method, Section IV describes public data exploited for validating the method, and Section V discusses the results.

II. Background

When dealing with EEG, artifact removal techniques can be classified into four main groups [12], [34]: regression-based, filtering, blind source separation, and source decomposition. In addition, new learning-based methods are recently receiving increasing attention [9], but these are beyond the present study.

Regression methods are still considered a gold standard, though they have been gradually replaced by more sophisticated methods. Meanwhile, *filtering methods* involve traditional frequency band-pass filters and adaptive ones. The former can be used if the bands of artifacts do not overlap with the signal of interest, while the latter are more flexible.

Simplicity and moderate computational costs are the main advantages of such techniques, while the need of a-priori knowledge and/or reference channels are their major drawbacks. In this context, a recent and promising adaptive filtering technique is the ASR [31]. ASR computes a covariance matrix and retrieves statistics to identify and remove short, high-amplitude artifact components (e.g., muscle artifacts) [35].

Other artifact removal techniques can be classified as *blind source separation methods* and *source decomposition methods*. They do not require reference channels nor a-priori knowledge about the artifacts, but they are based on strict assumptions of linearity, independence, and uncorrelation. In addition, they typically have high computational costs.

Blind source separation methods estimate a relationship matrix between the observed signals and the real unknown sources that generated them. The goal is to distinguish noise sources from real brain sources. Typical examples are the ICA, the CCA, or the principal component analysis (PCA). This category of techniques is often used in high-density biomedical signal processing [10], [30].

Source decomposition methods are based on the idea that the signal from each sensor can be decomposed into a series of fundamental modes in the time-frequency domain. Again, the noise components should be distinguishable in the transformed domain and removed before reconstructing the clean signal. Well-known examples are the wavelet transform [36] and the EMD [37]. In particular, EMD can only decompose one-dimensional signals independently. Meanwhile, the MEMD can decompose all the signals of a multi-dimensional acquisition at the same time by computing the same number of coherent modes for each sensor [38].

In a preliminary study [11], ICA, PCA, and ASR were compared while diminishing the number of available sensors. In accordance with literature, ASR appeared as the most effective and balanced method when exploiting at least four sensors. Indeed, ASR was able to effectively correct the physiological artifacts while preserving a large part of the pure EEG signal it was found to be the fastest technique (even 10 times faster than ICA). However, its performance was degraded with less than four sensors. For the above reasons, the following section deals with the enhancement of ASR by means of MEMD.

III. Proposed Method

The proposed method aims at enabling the usage of few EEG sensors. Similarly to literature hybrid approaches, the few available signals are decomposed before applying a multi-dimensional artifact removal technique. However, using MEMD for that purpose is relatively new and the combination with ASR was unexplored.

A. Design

MEMD decomposition operates in a multivariate time-frequency domain and it gives back basic waveforms called intrinsic mode functions (IMFs) [38]. Differently from EMD, the MEMD returns the same number of matched scale-aligned IMFs for each available signal. Artifacts could then be identified in the new space by applying ASR [31]. Notably, the ASR still relies on the statistics of a calibration interval, but retrieving statistics and cleaning must be done on IMFs.

In order to work properly, the MEMD and the ASR cannot be simply cascaded, but additional steps are necessary. Overall, the pipeline of the proposed hybrid method consists of five steps (Fig. 1):

1) preprocessing: the EEG signals are filtered in the frequency bands of interest and, after that, the epochs to analyze can be selected.

2) decomposition: the MEMD is carried out on all the available EEG signals simultaneously. The number of directions of the signal projection should be explicitly fixed. To extract meaningful IMFs, this number must be greater than the dimensionality of the original signal. The rule adopted in the current proposal is

$$N_{directions} = 2 \times (N_{sensors} + 1), \tag{1}$$

with the constraint of having at least six directions. This choice is consistent with the indications of the developers [39], [40]. At the decomposition end, the IMFs of each signal are matched among the corresponding sensors.

3) IMF grouping: the resulting IMFs have much different amplitudes, and this prevents direct application of ASR. Therefore, IMFs with low amplitudes are identified and summed to the last IMF with acceptable amplitude. To set an amplitude boundary, a calibration interval before decomposition is taken into account and the difference Δ_p between the 90^{th} and 10^{th} percentile is calculated for each sensor. Then, the same quantity is calculated for all the IMFs associated with that calibration interval. If the inter-quartile range of an IMF is lower than $10\,\%$ of Δ_p for at least one sensor, all the matched

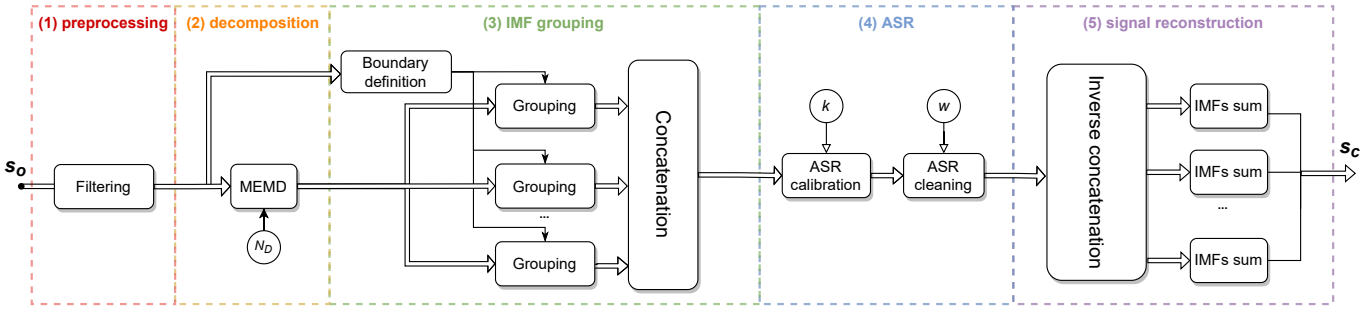

Fig. 1. Block diagram of the proposed hybrid method for artifact removal.

IMFs are summed up with the closest matched IMFs above the boundary. This process is done consistently for all sensors.

4) ASR: it includes a calibration phase and a cleaning phase. In this hybrid method, the calibration data are the IMFs obtained from the decomposition of the calibration interval. A mixing matrix M is obtained as the square root of the covariance matrix of calibration data. PCA is carried out for this mixing matrix. Then, a rejection threshold is automatically selected for each principal component as

$$\Gamma_i = \mu_i + k\sigma_i, \tag{2}$$

where μ_i and σ_i are the mean and standard deviation of the root mean square values obtained with a sliding window for each component. The threshold depends on the cut-off parameter k and the time window w on which statistics are calculated. For each window, the algorithm zeroes the components exceeding the rejection limit.

5) signal reconstruction: once the data are cleaned with the ASR, the signals in the original space are reconstructed by the inverse MEMD, i.e. the cleaned IMFs for each sensor are coherently summed up.

In the proposed method, calibration and artifacts data should be ideally recorded in compatible conditions, namely with the same acquisition hardware, in the same session, and with the same subject. However, calibration data from a previous session of the same subject could be re-used.

Moreover, this hybrid method can be also applied to multi-dimensional signals with any number of sensors. Nonetheless, it should be noted that the number of IMFs passed to the ASR grows exponentially as the number of sensors increases.

B. Implementation

The proposed MEMD-ASR method was implemented as a MATLAB© function, so that it can be easily integrated in EEG processing pipelines. The inputs of this function were:

- the *original signal* to be cleaned, expressed as a $(S \times N)$ matrix, where S is the number of samples and N is the number of sensors;
- the *sampling frequency* of the original signal, expressed in samples per second;
- the *calibration interval* corresponding to a time interval in which artifacts are assumed as absent;
- the *cut-off parameter of ASR*, expressed as an integer greater than one; it determines the aggressiveness of data rejection: the smaller the k, the more the aggressiveness.
- the *length of the statistics window*, expressed in seconds. This value w should be no longer than the time-duration of the artifacts [31].

The output consists of the cleaned signal, still expressed as a $(S \times N)$ matrix.

Inside the function, the five steps described above were implemented. During signal preparation, a chunk of signal had to be added at the end of the original signal. This typically consists of the last $0.25\,\mathrm{s}$ of the original signal that is flipped and concatenated. The reason is that the ASR cleaning function introduces a default delay due to a look-ahead operation. With this option, the ASR can reconstruct a sample by considering not only its preceding samples, but also the following ones [31]. Therefore, adding the chunk is needed whenever the look-ahead is exploited, while this will be removed in signal reconstruction by cutting the last $0.25\,\mathrm{s}$.

The function implementing the MEMD was taken from [39], where the output IMFs are given as a cell per each sensor. These cells were converted into matrices, with rows corresponding to IMFs. Then, the grouping criterion was applied to reduce the number of IMFs to be passed to the ASR. Finally, the resulting IMFs per sensor were concatenated in a unique matrix.

Overall, reduced IMFs were obtained for either the calibration interval and the epochs with artifacts. These were given in input to the ASR, where the calibration function returns a state for initializing the subsequent cleaning phase. In addition to the state, the inputs for the cleaning phase are the data matrix, the sampling rate, the window length, and the look-ahead value. At the end of cleaning, the signal is reconstructed by summing the IMFs per sensor.

IV. Datasets

The proposed method was validated on public semi-synthetic and experimental datasets. Compared to purely synthetic data, semi-synthetic data offer more realistic signal variability and power, ensuring reliability and results significance. To generate semi-synthetic data, pure EEG data were first synthesized and then partially contaminated with artifacts extracted from real recordings. In doing so, the pure EEG can be easily compared with the cleaned EEG. This is indeed not possible with actual EEG data, but the results on them should be discussed differently.

TABLE I
CORRELATION COEFFICIENTS TO WEIGHT OCULAR ARTIFACTS AND EYE BLINKING FOR EACH SENSOR.

Channel	Fp1	Fp2	F7	F3	Fz	F4	F8	C3	Cz	C4	P7	Pz	P8	O1	O2
Weight	0.87	1.00	0.59	0.25	0.73	0.44	0.47	0.24	0.00	0.12	0.35	0.26	0.27	0.31	0.28

A. Semi-synthetic data

Pure EEG signals were synthesized with the recently developed *SEED-G simulator* available online [41]. Per each sensor, a $150\,\mathrm{s}$-long pure signal was generated with a sampling frequency of $256\,\mathrm{Sa/s}$. These parameters were chosen in order to have suitable data for the application of the ASR. In detail, the first $60\,\mathrm{s}$ of the trace were left intact to represent clean calibration data. The remaining $90\,\mathrm{s}$ were contaminated with three types of artifacts: muscular, ocular, and eye blinking.

The muscular and ocular artifacts were extracted from the online *DenoiseNet database* [42]. These artifacts are available in $2\,\mathrm{s}$-long segments at a sampling rate of $256\,\mathrm{Sa/s}$, consistent with the choice made to simulate pure EEG. Therefore, 15 segments were randomly extracted for each artifact type to obtain $30\,\mathrm{s}$ of muscular artifacts and $30\,\mathrm{s}$ of ocular artifacts. In addition, eye blinking artifacts were added on the last $30\,\mathrm{s}$ of the signal. In this case, half sinusoidal signals with $0.2\,\mathrm{s}$ duration were added to simulate the typical eye blinking peaks. The time distance between them was set $1\,\mathrm{s}$ apart.

The amplitude of the synthetic artifacts was adjusted with respect to the pure synthetic signal to achieve a signal-to-noise ratio (SNR) from $-20\,\mathrm{dB}$ to $5\,\mathrm{dB}$ [43]. Moreover, since ocular artifacts and eye blinking usually propagate over the scalp starting from the prefrontal area, their addition was weighted per channel. The weights were achieved as the correlation coefficients between real electrooculographic data and corresponding EEG data [41]. Fifteen channels were thus chosen from different regions of the scalp, and these are indicated in Tab. I with the mentioned correlation coefficients.

B. Experimental data from a public dataset

A public dataset was exploited to extract actual EEG data [44]. This dataset is meant for testing artifact removal techniques and includes 13 participants with one recording session each. Brain signals were recorded by using a helmet by Brain Products [45] with 27 EEG channels and 3 electrooculographic channels, at a sampling rate of $200\,\mathrm{Sa/s}$. Despite the non-wearability of the acquisition device, these publicly available data were chosen for the sake of reproducibility and the possibility to analyze different numbers of sensors. The subjects sat in front of a screen to follow instructions for performing muscular or ocular artifacts.

Each experimental session consisted of two parts. First the subjects were asked to focus on a fixation cross on the screen and avoid doing artifacts (baseline). Clean $30\,\mathrm{s}$-long signals were thus recorded for each subject twice. Secondly, nine different artifact types were done in random order for 10 times each. A single trial with artifact lasted from $10\,\mathrm{s}$ to $30\,\mathrm{s}$, for a total length of $40\,\mathrm{min}$ to $50\,\mathrm{min}$ for the second part.

In the present work, data from the first subject of the dataset were chosen to be processed. For computational reasons, the length of the entire EEG signal was limited to about $8\,\mathrm{min}$. While the two sets of baseline signals were kept unchanged, only 10 continuous artifact conditions were considered for the contaminated signal part. Finally, the whole EEG data were filtered in the $1\,\mathrm{Hz}$ to $40\,\mathrm{Hz}$ range and base-normalized to have zero mean. Note that the last condition was also satisfied when generating semi-synthetic data.

V. RESULTS AND DISCUSSION

The experimental setup is described in this section along with the metrics adopted for quantifying the method's effectiveness. The results presented hereafter can be reproduced by exploiting the code published at https://github.com/anthonyesp/low_density_eeg_asr.git.

A. Experimental setup

In accordance with the above discussion, the proposed hybrid method was tested from four sensors down to a single sensor. Notably, in the case of a single sensor, the MEMD is actually an EMD. Per each number of sensors, the sensors were randomly selected 15 times among available ones to obtain an average performance independently of their locations.

Different values for the cut-off parameter k and for the statistical window w associated with ASR were investigated to identify the best pair. Notably, k was varied from 5 to 30 with step 1 and w was varied from $0.2\,\mathrm{s}$ to $3.0\,\mathrm{s}$ with step $0.1\,\mathrm{s}$. The selection of the best ASR parameters was based on the relative root mean square error (RRMSE) [46]. It reflects the differences between the pure EEG signal and the EEG signal cleaned by MEMD-ASR. It is defined as:

$$RRMSE = \sqrt{\frac{\sum_{i=1}^{N} \left[eeg^{\star}(i) - eeg(i)\right]^2}{\sum_{i=1}^{N} eeg(i)^2}}, \tag{3}$$

where $eeg(i)$ and $eeg^{\star}(i)$ are samples of the uncontaminated signal and cleaned one, respectively. These values should be zero in the ideal case, i.e. with artifacts perfectly removed.

Therefore, semi-synthetic data were primarily used in these tests. RRMSE was calculated on different segments: the segment used as baseline for ASR, the residual pure EEG (not used as baseline), the segments with muscle artifacts, the one with ocular artifacts, and the one with blink artifacts.

The point defined by the five RRMSE values (as five were the EEG segments) was considered in an Euclidean 5D space and its norm was calculated. The dispersion around these values was also taken into account and propagated to achieve the uncertainty of the norm. The optimal w was chosen to minimize the Euclidean norm and possibly its associated uncertainty. Then, a k was identified by looking for the minimum 90^{th} percentile associated with the five values. As an

essential check, once w and k were fixed, a visual inspection of the signals in the time domain was carried on. In particular, the pure signal and the signal cleaned with MEMD-ASR were compared for each segment of the EEG signal.

Eventually, the hybrid method was tested on experimental data by using the best w and k chosen on semi-synthetic data. Again, sensors were randomly selected 15 times from the available ones to test the method from four sensors down to a single sensor. In order to evaluate the effectiveness of the hybrid method on experimental data, a visual inspection of the signals in the time domain was carried out. The RRMSE was calculated too. Nonetheless, as the pure signal is not available with experimental data, this metric has the same meaning of the semi-synthetic data case only when considering the baseline and pure segments. The same metric was calculated on the remaining segments with artifacts are thus not reported to avoid misunderstandings.

B. Results on semi-synthetic data

To identify the optimal k and w values, Fig. 2 shows the Euclidean 5D norm associated with median RRMSE values. Moreover, its colours refer to the dispersion of the norm. This specific result regards the two-sensors case, but similar surfaces were obtained in the other cases.

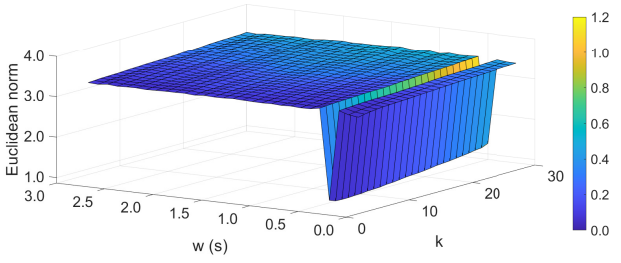

Fig. 2. Surface obtained by calculating the Euclidean norm in 5D space associated with the RRMSE in the two-sensors case.

As observed by the sharp negative peak, $w = 0.5\,\mathrm{s}$ remained unaffected by both the k value and the number of sensors. This w value corresponds to the default length of the statistics window [31], [47]. In addition, a value for k in the 5 to 10 range minimizes both the norm and its dispersion. After fixing w, the optimal value of k was identified as described in V-A per each number of sensors. In general, for small k values, the baseline and pure segments differ from the original ones, but the artifacts are completely removed. On the other hand, for large k values, the baseline and pure segments match the original ones but the artifacts are only partially removed.

Tab. II reports the median RRMSE corresponding to the optimal w and k values. Moreover, the novel hybrid method was compared to ASR and MEMD alone. Note that the classical ASR cannot be applied to a single sensor as a method based on co-variance [48], [49], thus EMD-ASR was only compared with EMD alone. Furthermore, entropy was used as a criterion to identify and remove artifactual IMFs, as proposed in [50]. These results demonstrate that the proposed hybrid method performs compatibly with the ASR. In contrast, the only MEMD is not effective in isolating artifacts but, due to its filter bank-like behaviour [38], it affects clean signals.

TABLE II
MEDIAN RRMSE VALUES FOR SEMI-SYNTHETIC DATA.

#sensors	method	w (s)	k	baseline	pure	muscle	ocular	blinks
4	MEMD	-	-	0.00	0.00	8.61	0.99	0.56
4	ASR	0.5	7	0.00	0.00	0.27	0.34	0.40
4	MEMD-ASR	0.5	9	0.00	0.00	0.60	0.30	0.46
3	MEMD	-	-	0.18	0.20	8.87	0.95	0.59
3	ASR	0.5	8	0.00	0.00	0.38	0.37	0.47
3	MEMD-ASR	0.5	8	0.01	0.00	0.70	0.34	0.45
2	MEMD	-	-	0.25	0.27	9.08	0.90	0.54
2	ASR	0.5	12	0.00	0.00	0.69	0.58	0.55
2	MEMD-ASR	0.5	9	0.00	0.00	0.70	**0.35**	0.45
1	EMD	-	-	0.27	0.31	9.24	0.65	0.62
1	EMD-ASR	0.5	12	0.00	0.00	1.25	0.50	0.59

bold: median RRMSE for MEMD-ASR significantly lower than respective ASR one.
w: length of the statistics window in seconds; k: cut-off parameter of ASR.

The RRMSE values of Tab II are also compatible with previous studies. Notably, by considering results on semi-simulated data with an SNR between $-20\,\mathrm{dB}$ to $5\,\mathrm{dB}$, the RRMSE values reported in [20]–[22] span in the 0.2 to 0.5 range. Moreover, it should be noted that the minimum number of considered channels was 3, even when taking into account other relevant studies [24], [40].

The Mann-Whitney U-test [51] was applied to prove differences between MEMD-ASR, ASR, and MEMD with a $5\,\%$ significance level. The test results confirmed that the medians of RRMSE for ASR are not significantly different from MEMD-ASR, except for the case of ocular artifact with two sensors (reported in bold). Meanwhile, they also confirmed that MEMD performs worse than both MEMD-ASR and ASR.

The gain in signal-to-artifact ratio (γ) [46] was then investigated as a further metric. Notably, this could be only exploited on semi-synthetic data as it requires the availability of the true EEG. The γ is defined as

$$\gamma = 10 \log \frac{\sum_{n=1}^{N} |eeg^{\diamond}(i) - eeg(i)|^2}{\sum_{n=1}^{N} |eeg^{\star}(i) - eeg(i)|^2}, \tag{4}$$

where $eeg^{\diamond}(i)$ are the samples of the contaminated EEG signal. Positive values of gamma indicate a better signal-to-noise ratio, negative values indicate a decrease, while zero represents no improvement. Tab. III reports the median γ, corresponding to the optimal w and k values, in comparing the novel hybrid method with ASR and MEMD alone.

TABLE III
MEDIAN γ VALUES FOR SEMI-SYNTHETIC DATA.

#sensors	method	w (s)	k	muscle	ocular	blinks
4	MEMD	-	-	0.00	0.00	0.00
4	ASR	0.5	7	29.70	12.66	6.33
4	MEMD-ASR	0.5	9	23.85	13.63	5.37
3	MEMD	-	-	0.50	1.64	0.76
3	ASR	0.5	8	27.12	12.41	4.84
3	MEMD-ASR	0.5	8	22.64	12.88	5.40
2	MEMD	-	-	0.95	0.63	0.54
2	ASR	0.5	12	22.47	5.37	0.00
2	MEMD-ASR	0.5	9	21.01	**9.58**	**1.85**
1	EMD	-	-	1.07	5.03	2.19
1	EMD-ASR	0.5	12	16.31	6.50	0.00

bold: median γ for MEMD-ASR significantly higher than respective ASR one.
w: length of the statistics window in seconds; k: cut-off parameter of ASR.

Since the contaminated signal $eeg^{\diamond}(i)$ and the uncontaminated signal $eeg(i)$ coincide within the baseline and pure segments, γ was computed only for the three artifact conditions. Also in this case, statistical testing proved the superior performance of MEMD-ASR over ASR for eye blinks, but also for ocular artifacts, in the two sensors case. In all other cases, MEMD-ASR and ASR demonstrated compatible performance and both were better than only MEMD.

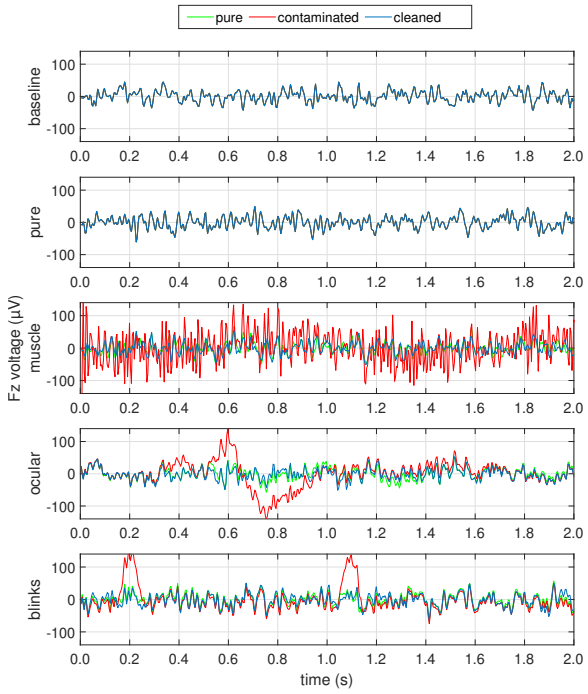

Fig. 3. Visual inspection of the sensor Fz with two sensors involved in artifact removal by MEMD-ASR. Quantitative metrics associated with these semi-synthetic data are reported in Tab. II and Tab. III.

Visual inspection confirmed that MEMD-ASR and ASR have compatible performance on these data. Meanwhile, EMD-ASR is effective in removing ocular and eye-blink artifacts on single-channel EEG. Fig. 3 shows a representative example of visual inspection. The two-sensors case was considered and the sensor Fz is here represented with respect to the five EEG segments. As expected, the green (pure signal) and the blue (signal cleaned with MEMD-ASR) curves are mostly overlapped. Hence, artifacts are removed with respect to the red curves representing contaminated signals.

C. Results on experimental data from the public dataset

As anticipated, the optimal w and k values derived with the semi-synthetic data were adopted on experimental data too. Tab. IV reports, for the only baseline and pure data segments, the median RRMSE corresponding to the same w and k values of Tab. II. The novel method was again compared to MEMD and ASR. The proposed hybrid method affects the baseline and the pure signal segment less than both MEMD and ASR alone, with a significant difference for all cases from 4 to 2 sensors.

An example of the effectiveness of MEMD-ASR in removing artifacts is reported in Fig. 4. The two-sensors case was

TABLE IV
MEDIAN RRMSE FOR EXPERIMENTAL DATA

#sensors	method	w (s)	k	baseline	pure
4	MEMD	-	-	0.94	0.94
4	ASR	0.5	7	0.90	0.90
4	MEMD-ASR	0.5	9	**0.32**	**0.28**
3	MEMD	-	-	1.01	1.01
3	ASR	0.5	8	1.14	1.14
3	MEMD-ASR	0.5	8	**0.34**	**0.40**
2	MEMD	-	-	0.80	0.75
2	ASR	0.5	12	0.94	0.98
2	MEMD-ASR	0.5	9	**0.19**	**0.28**
1	EMD	-	-	0.72	0.67
1	EMD-ASR	0.5	12	0.18	0.15

bold: median RRMSE for MEMD-ASR significantly lower than respective ASR. w: length of the statistics window in seconds; k: cut-off parameter of ASR.

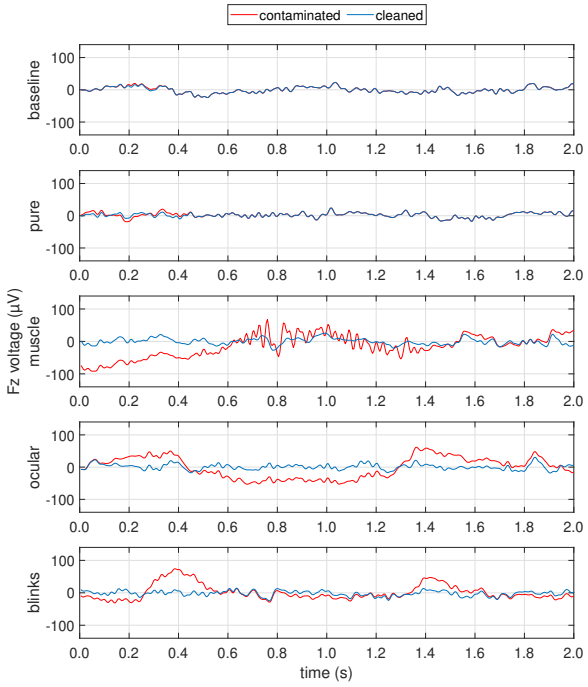

Fig. 4. Visual inspection of the sensor Fz with two sensors involved in artifact removal by MEMD-ASR. Quantitative metrics associated with these experimental data are reported in Tab. IV.

considered and the sensor Fz is here represented with respect to the five EEG segments. The signals cleaned with MEMD-ASR (blue) are here compared to the experimental data signals (red). It can be seen that these signals are mostly overlapped in the baseline and pure conditions, while artifacts are removed in the other three conditions.

The effectiveness of the proposed methods is furtherly supported by the visual inspection of baseline and ocular artifacts for comparing the artifact removal methods (Fig. 5). In there, the two-sensors case was again involved. In the calibration segment neither MEMD nor MEMD-ASR affects the signal, while the ASR already disrupts it. Regarding the noisy segment, the MEMD-ASR is the only to effectively remove ocular artifacts. Conversely, the MEMD fails to mitigate artifacts and the ASR overcorrects them. Indeed, the ASR fails to remove artifacts and cancels out the signal on experimental data, in contrast to its performance on semi-synthetic data.

In concluding, it should be noted that a drawback of the

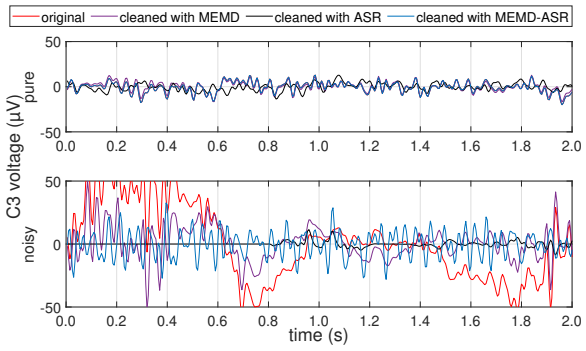

Fig. 5. Visual inspection of the sensor C3 with two sensors involved in comparing artifact removal methods. Quantitative metrics associated with these experimental data are reported in Tab. IV.

proposed technique is execution time. ASR alone takes about $0.2\,\mathrm{s}$ to $0.4\,\mathrm{s}$ to remove artifacts, where the more the sensor the higher the time. Meanwhile, MEMD-ASR execution takes from about $32\,\mathrm{s}$ (two sensors) to about $72\,\mathrm{s}$ (four sensors). Instead, EMD-ASR for a single sensor takes about $0.7\,\mathrm{s}$. The multivariate EMD thus creates a bottleneck in terms of processing time, but the EMD-ASR discloses the possibility to implement a soft EEG sensor with integrated artifact removal features.

D. From semi-synthetic to experimental data

Results on semi-synthetic data suggest that ASR is equally or more effective than MEMD-ASR down to two sensors. Meanwhile, a significant improvement with MEMD-ASR holds for the removal of ocular artifacts in two sensors case. This was confirmed with statistical testing on both RRMSE and γ metrics. In contrast, MEMD alone was always found to be less effective than ASR and MEMD-ASR. Compared with ASR alone, the proposed method discloses the possibility to work on a single sensor. However, EMD-ASR does not seem effective in removing blinks.

Conversely, when experimental data were used, the MEMD-ASR appeared more effective than ASR and MEMD in not affecting the baseline and pure EEG signal. Furthermore, the visual inspection in Fig. 4 proves that the hybrid approach exhibits a balanced corrective action. Meanwhile, in accordance with literature [38], MEMD fails to remove artifacts in the same frequency bands of the signal.

Finally, Fig. 5 supports the importance of testing artifact removal techniques on experimental data despite the unknown pure EEG. Notably, the only RRMSE would not highlight the issue, thus confirming the importance of visual inspection in the current scenario.

VI. Conclusion

This work has proposed a hybrid artifact removal method addressed to low-density EEG. Differently from existing literature, this was designed to remove various types of EEG artifacts and to jointly consider all the available channels for maximizing the available information. The method relies on the multivariate version of EMD and on ASR.

Both semi-synthetic and experimental data were exploited to validate the method. In the former case, the hybrid method has performance compatible with the classical ASR.In the latter case, visual inspection demonstrated that ASR is not effective on experimental data, while only MEMD-ASR works properly. This also suggested that semi-synthetic data are not always appropriate to test artifact removal techniques. Finally, MEMD was found to be less effective than MEMD-ASR and ASR.

Future works should furtherly explore the applicability of the proposed methods in different settings. Moreover, execution time should also be reduced if willing to realize soft sensors for online applications. Finally, a standardization in terms of metric is still required, especially when experimental data are used. These speculations will be eased by the material shared for the present paper to replicate and extend the results.

References

[1] M. Teplan *et al.*, "Fundamentals of EEG measurement," *Measurement science review*, vol. 2, no. 2, pp. 1–11, 2002.

[2] J. S. Kumar and P. Bhuvaneswari, "Analysis of Electroencephalography (EEG) signals and its categorization–a study," *Procedia engineering*, vol. 38, pp. 2525–2536, 2012.

[3] P. Arpaia, E. De Benedetto, C. A. Dodaro, L. Duraccio, and G. Servillo, "Metrology-based design of a wearable augmented reality system for monitoring patient's vitals in real time," *IEEE Sensors Journal*, vol. 21, no. 9, pp. 11176–11183, 2021.

[4] P. Arpaia, E. De Benedetto, L. De Paolis, G. D'Errico, N. Donato, and L. Duraccio, "Performance enhancement of wearable instrumentation for AR-based SSVEP BCI," *Measurement*, vol. 196, p. 111188, 2022.

[5] A. Apicella, P. Arpaia, E. De Benedetto, N. Donato, L. Duraccio, S. Giugliano, and R. Prevete, "Enhancement of SSVEPs classification in BCI-based wearable instrumentation through machine learning techniques," *IEEE Sensors Journal*, vol. 22, no. 9, pp. 9087–9094, 2022.

[6] A. E. Hramov, V. A. Maksimenko, and A. N. Pisarchik, "Physical principles of brain–computer interfaces and their applications for rehabilitation, robotics and control of human brain states," *Physics Reports*, vol. 918, pp. 1–133, 2021.

[7] P. Arpaia, L. Callegaro, A. Cultrera, A. Esposito, and M. Ortolano, "Metrological characterization of consumer-grade equipment for wearable brain–computer interfaces and extended reality," *IEEE Transactions on Instrumentation and Measurement*, vol. 71, pp. 1–9, 2021.

[8] P. Sawangjai, S. Hompoonsup, P. Leelaarporn, S. Kongwudhikunakorn, and T. Wilaiprasitporn, "Consumer grade EEG measuring sensors as research tools: A review," *IEEE Sensors Journal*, vol. 20, no. 8, pp. 3996–4024, 2019.

[9] J. Minguillon, M. A. Lopez-Gordo, and F. Pelayo, "Trends in EEG-BCI for daily-life: Requirements for artifact removal," *Biomedical Signal Processing and Control*, vol. 31, pp. 407–418, 2017.

[10] W. Mumtaz, S. Rasheed, and A. Irfan, "Review of challenges associated with the EEG artifact removal methods," *Biomedical Signal Processing and Control*, vol. 68, p. 102741, 2021.

[11] P. Arpaia, E. De Benedetto, A. Esposito, A. Natalizio, M. Parvis, and M. Pesola, "Comparing artifact removal techniques for daily-life electroencephalography with few channels," in *2022 IEEE International Symposium on Medical Measurements and Applications (MeMeA)*, pp. 1–6, IEEE, 2022.

[12] J. A. Urigüen and B. Garcia-Zapirain, "EEG artifact removal—state-of-the-art and guidelines," *Journal of neural engineering*, vol. 12, no. 3, p. 031001, 2015.

[13] A.-O. Boudraa and J.-C. Cexus, "Emd-based signal filtering," *IEEE transactions on instrumentation and measurement*, vol. 56, no. 6, pp. 2196–2202, 2007.

[14] A. Komaty, A.-O. Boudraa, B. Augier, and D. Daré-Emzivat, "Emd-based filtering using similarity measure between probability density functions of imfs," *IEEE Transactions on Instrumentation and Measurement*, vol. 63, no. 1, pp. 27–34, 2013.

[15] Z. Wu and N. E. Huang, "Ensemble empirical mode decomposition: a noise-assisted data analysis method," *Advances in adaptive data analysis*, vol. 1, no. 01, pp. 1–41, 2009.

[16] P. Gaur, R. B. Pachori, H. Wang, and G. Prasad, "An automatic subject specific intrinsic mode function selection for enhancing two-class eeg-based motor imagery-brain computer interface," *IEEE Sensors Journal*, vol. 19, no. 16, pp. 6938–6947, 2019.

[17] O. A. Omitaomu, V. A. Protopopescu, and A. R. Ganguly, "Empirical mode decomposition technique with conditional mutual information for denoising operational sensor data," *IEEE sensors journal*, vol. 11, no. 10, pp. 2565–2575, 2011.

[18] K. Zeng, D. Chen, G. Ouyang, L. Wang, X. Liu, and X. Li, "An EEMD-ICA approach to enhancing artifact rejection for noisy multivariate neural data," *IEEE transactions on neural systems and rehabilitation engineering*, vol. 24, no. 6, pp. 630–638, 2015.

[19] X. Chen, A. Liu, J. Chiang, Z. J. Wang, M. J. McKeown, and R. K. Ward, "Removing muscle artifacts from eeg data: Multichannel or single-channel techniques?," *IEEE Sensors Journal*, vol. 16, no. 7, pp. 1986–1997, 2015.

[20] X. Xu, A. Liu, and X. Chen, "A novel few-channel strategy for removing muscle artifacts from multichannel EEG data," in *2017 IEEE Global Conference on Signal and Information Processing (GlobalSIP)*, pp. 976–980, IEEE, 2017.

[21] X. Chen, X. Xu, A. Liu, M. J. McKeown, and Z. J. Wang, "The use of multivariate EMD and CCA for denoising muscle artifacts from few-channel EEG recordings," *IEEE transactions on instrumentation and measurement*, vol. 67, no. 2, pp. 359–370, 2017.

[22] Y. Liu, Y. Zhou, X. Lang, Y. Liu, Q. Zheng, Y. Zhang, X. Jiang, L. Zhang, J. Tang, and Y. Dai, "An efficient and robust muscle artifact removal method for few-channel EEG," *IEEE Access*, vol. 7, pp. 176036–176050, 2019.

[23] X. Lang, Q. Zheng, Z. Zhang, S. Lu, L. Xie, A. Horch, and H. Su, "Fast multivariate empirical mode decomposition," *IEEE Access*, vol. 6, pp. 65521–65538, 2018.

[24] G. Wang, C. Teng, K. Li, Z. Zhang, and X. Yan, "The removal of eog artifacts from eeg signals using independent component analysis and multivariate empirical mode decomposition," *IEEE journal of biomedical and health informatics*, vol. 20, no. 5, pp. 1301–1308, 2015.

[25] N. K. Al-Qazzaz, S. Hamid Bin Mohd Ali, S. A. Ahmad, M. S. Islam, and J. Escudero, "Automatic artifact removal in eeg of normal and demented individuals using ica–wt during working memory tasks," *Sensors*, vol. 17, no. 6, p. 1326, 2017.

[26] X. Chen, Q. Chen, Y. Zhang, and Z. J. Wang, "A novel eemd-cca approach to removing muscle artifacts for pervasive eeg," *IEEE Sensors Journal*, vol. 19, no. 19, pp. 8420–8431, 2018.

[27] R. Ranjan, B. C. Sahana, and A. K. Bhandari, "Ocular artifact elimination from electroencephalography signals: A systematic review," *Biocybernetics and Biomedical Engineering*, vol. 41, no. 3, pp. 960–996, 2021.

[28] A. K. Maddirala and R. A. Shaik, "Removal of eog artifacts from single channel eeg signals using combined singular spectrum analysis and adaptive noise canceler," *IEEE Sensors Journal*, vol. 16, no. 23, pp. 8279–8287, 2016.

[29] R. Patel, M. P. Janawadkar, S. Sengottuvel, K. Gireesan, and T. S. Radhakrishnan, "Suppression of eye-blink associated artifact using single channel eeg data by combining cross-correlation with empirical mode decomposition," *IEEE Sensors Journal*, vol. 16, no. 18, pp. 6947–6954, 2016.

[30] C. Stergiadis, V.-D. Kostaridou, and M. A. Klados, "Which BSS method separates better the EEG Signals? A comparison of five different algorithms," *Biomedical Signal Processing and Control*, vol. 72, p. 103292, 2022.

[31] T. R. Mullen, C. A. Kothe, Y. M. Chi, A. Ojeda, T. Kerth, S. Makeig, T.-P. Jung, and G. Cauwenberghs, "Real-time neuroimaging and cognitive monitoring using wearable dry EEG," *IEEE Transactions on Biomedical Engineering*, vol. 62, no. 11, pp. 2553–2567, 2015.

[32] S. Blum, N. S. Jacobsen, M. G. Bleichner, and S. Debener, "A riemannian modification of artifact subspace reconstruction for eeg artifact handling," *Frontiers in human neuroscience*, vol. 13, p. 141, 2019.

[33] A. Cataldo, S. Criscuolo, E. De Benedetto, A. Masciullo, M. Pesola, R. Schiavoni, and S. Invitto, "A method for optimizing the artifact subspace reconstruction performance in low-density eeg," *IEEE Sensors Journal*, vol. 22, no. 21, pp. 21257–21265, 2022.

[34] K. Zeng and X. Li, "Artifact Removal in EEG Recordings," in *Signal Processing in Neuroscience*, pp. 77–98, Springer, 2016.

[35] X. Chen, X. Xu, A. Liu, S. Lee, X. Chen, X. Zhang, M. J. McKeown, and Z. J. Wang, "Removal of muscle artifacts from the eeg: A review and recommendations," *IEEE Sensors Journal*, vol. 19, no. 14, pp. 5353–5368, 2019.

[36] M. Unser and A. Aldroubi, "A review of wavelets in biomedical applications," *Proceedings of the IEEE*, vol. 84, no. 4, pp. 626–638, 1996.

[37] N. E. Huang, Z. Shen, S. R. Long, M. C. Wu, H. H. Shih, Q. Zheng, N.-C. Yen, C. C. Tung, and H. H. Liu, "The empirical mode decomposition and the hilbert spectrum for nonlinear and non-stationary time series analysis," *Proceedings of the Royal Society of London. Series A: mathematical, physical and engineering sciences*, vol. 454, no. 1971, pp. 903–995, 1998.

[38] D. P. Mandic, N. Ur Rehman, Z. Wu, and N. E. Huang, "Empirical mode decomposition-based time-frequency analysis of multivariate signals: The power of adaptive data analysis," *IEEE signal processing magazine*, vol. 30, no. 6, pp. 74–86, 2013.

[39] Y. Zhang, P. Xu, P. Li, K. Duan, Y. Wen, Q. Yang, T. Zhang, and D. Yao, "Noise-assisted multivariate empirical mode decomposition for multichannel EMG signals," *Biomedical engineering online*, vol. 16, no. 1, pp. 1–17, 2017.

[40] Y. Zhang, P. Xu, P. Li, K. Duan, Y. Wen, Q. Yang, T. Zhang, and D. Yao, "Noise-assisted multivariate empirical mode decomposition for multichannel emg signals," *Biomedical engineering online*, vol. 16, no. 1, pp. 1–17, 2017.

[41] A. Anzolin, J. Toppi, M. Petti, F. Cincotti, and L. Astolfi, "SEED-G: simulated EEG data generator for testing connectivity algorithms," *Sensors*, vol. 21, no. 11, p. 3632, 2021.

[42] "EEGdenoiseNet." https://github.com/ncclabsustech/EEGdenoiseNet. Last access: 2022-08.

[43] M. Dora and D. Holcman, "Adaptive single-channel eeg artifact removal with applications to clinical monitoring," *IEEE Transactions on Neural Systems and Rehabilitation Engineering*, vol. 30, pp. 286–295, 2022.

[44] S. Ehrlich. https://github.com/stefan-ehrlich/dataset-automaticArtifactRemoval. Last access: 2022-08.

[45] "Introducing the actichamp plus – offering active and passive electrode recordings … and more!." https://pressrelease.brainproducts.com/actichamp_plus/. Last access: 2022-08.

[46] M. M. N. Mannan, M. A. Kamran, and M. Y. Jeong, "Identification and removal of physiological artifacts from electroencephalogram signals: A review," *IEEE Access*, vol. 6, pp. 30630–30652, 2018.

[47] "Clean_rawdata EEGLAB plug-in." https://github.com/sccn/clean_rawdata. Last access: 2022-08.

[48] C.-Y. Chang, S.-H. Hsu, L. Pion-Tonachini, and T.-P. Jung, "Evaluation of artifact subspace reconstruction for automatic artifact components removal in multi-channel eeg recordings," *IEEE Transactions on Biomedical Engineering*, vol. 67, no. 4, pp. 1114–1121, 2019.

[49] V. P. Kumaravel, V. Kartsch, S. Benatti, G. Vallortigara, E. Farella, and M. Buiatti, "Efficient artifact removal from low-density wearable eeg using artifacts subspace reconstruction," in *2021 43rd Annual International Conference of the IEEE Engineering in Medicine & Biology Society (EMBC)*, pp. 333–336, IEEE, 2021.

[50] Q. Liu, Y.-F. Chen, S.-Z. Fan, M. F. Abbod, and J.-S. Shieh, "Eeg artifacts reduction by multivariate empirical mode decomposition and multiscale entropy for monitoring depth of anaesthesia during surgery," *Medical & biological engineering & computing*, vol. 55, 2017.

[51] P. E. McKnight and J. Najab, "Mann-whitney u test," *The Corsini encyclopedia of psychology*, pp. 1–1, 2010.

Pasquale Arpaia (Senior Member, IEEE) received the M.S. and Ph.D. degrees in electrical engineering from the University of Napoli Federico II in 1988 and 1992, respectively. He is a Full Professor of instrumentation and measurements with the University of Napoli Federico II.

Antonio Esposito (IEEE Member) received the M.S. in electronic engineering from the University of Naples Federico II in 2017 and the Ph.D. degree in Metrology from the Politecnico di Torino in 2022. His research activities focus on wearable brain-computer interfaces.

Angela Natalizio (IEEE Member) received the M.S. degree in biomedical engineering from the University of Naples Federico II in 2019. She is Ph.D. student in Metrology at the Politecnico di Torino. Her research activities focus on motor imagery-based brain-computer interfaces.

Marco Parvis (Fellow Member, IEEE) received his M.S. degree in electrical engineering in 1982 and a Ph.D. degree in Metrology in 1987 from the Politecnico di Torino, Italy. He is a Full Professor of electronic Measurements at the Politecnico di Torino.

Marisa Pesola received her M.S. degree in biomedical engineering at the University of Napoli Federico II in 2022, where she is currently a Ph.D. student in computational and quantitative biology. Her research interests focus on processing of biomedical signals and artifact removal.